Circuit and Electromagnetic System Design Notes

Note 63

January 2010

Microwave Pulse Compression Experiments at Low and High Power

E. G. Farr*, L. H. Bowen*, W. D. Prather**, and C. E. Baum***

*Farr Research, Inc., Albuquerque, NM, 87123
**Air Force Research Laboratory, Directed Energy Directorate,
Kirtland Air Force Base, NM 87117-5776
***University of New Mexico, Albuquerque, NM 87131-0001

Abstract

We describe here experiments that develop the technique of Microwave Pulse Compression (MPC). This is a method of concentrating and amplifying the power of a microwave pulse by reducing its duration. The technique involves exciting a resonant cavity with a microwave source, and then firing a shorting switch that destroys the resonance condition. The compressed pulse is then delivered to the output port at a higher peak power and smaller pulse width than the original microwave pulse. To demonstrate the technique, we built two MPCs operating at 1.3 GHz, one operating at low power, and the other at high power. In our low-power MPC we amplified 1 kW up to 33 kW, at a repetition rate of 10-50 Hz. In our high-power MPC, we amplified 2.8 MW up to 50 MW, at a repetition rate of 5-160 Hz. All of our switches were gas switches with trigatrons, filled with either evacuated air (10-13 mTorr) at low power, or 20 psig sulfur hexafluoride.

CONTENTS

I. Introduction

We describe here experiments to develop the technique of Microwave Pulse Compression (MPC). This is a method of concentrating and amplifying the power of a microwave pulse by reducing its duration. It is thought that this technique may be of use as a microwave source for vulnerability testing.

MPC involves exciting a resonant cavity with a microwave source, and then firing a shorting switch that destroys the resonance condition. The compressed pulse is then delivered to the output port at a higher peak power and smaller pulse width than the original microwave pulse.

Pulse compression has been used quite commonly at X-band and higher frequencies [1,2], but there are relatively few instances near 1 GHz [3,4,5]. The frequency spectrum near 1 GHz is of particular interest because it is most capable of upsetting and/or damaging electronics. In [6], D. P. Byrne describes in detail his MPC experiments at 2.9 GHz. In [7], C. E. Baum suggested pulse compression as a technique for implementing a microwave weapon. In [8], Baum presented a novel magic tee design that may be of use in pulse compression systems, due to its improved impedance match. In [9], Baum suggests some novel coupling schemes that will be of interest.

To demonstrate the technique, we built two MPCs operating at 1.3 GHz, one operating at low power, and the other at high power. In our low-power MPC we amplified 1 kW up to 33 kW, at a repetition rate of 10-50 Hz. In our high-power MPC, we amplified 2.8 MW up to 50 MW, at a repetition rate of 5-160 Hz. All of our switches were triggered gas switches with trigatrons, filled with either low-pressure air (~10-13 mTorr) at low power, or ~20 psig SF_6 at high power.

We begin with a description of the microwave pulse compression technique. We then describe our experiments at low and high power. Finally, we describe a series of possible improvements to increase the gain and make the cavity tunable.

II. Overview of Microwave Pulse Compression

A. The Concept

A sketch of a Microwave Pulse Compressor is shown in Figure 1. Power is pumped into a waveguide resonant length of rectangular waveguide whose length is an integral number of half guide wavelengths. The cavity is bounded at the input by an inductive iris, and at the output with an H-plane tee with sliding short. After power has built up, a switch is fired that destroys the cavity resonance, and the power exits at the output.

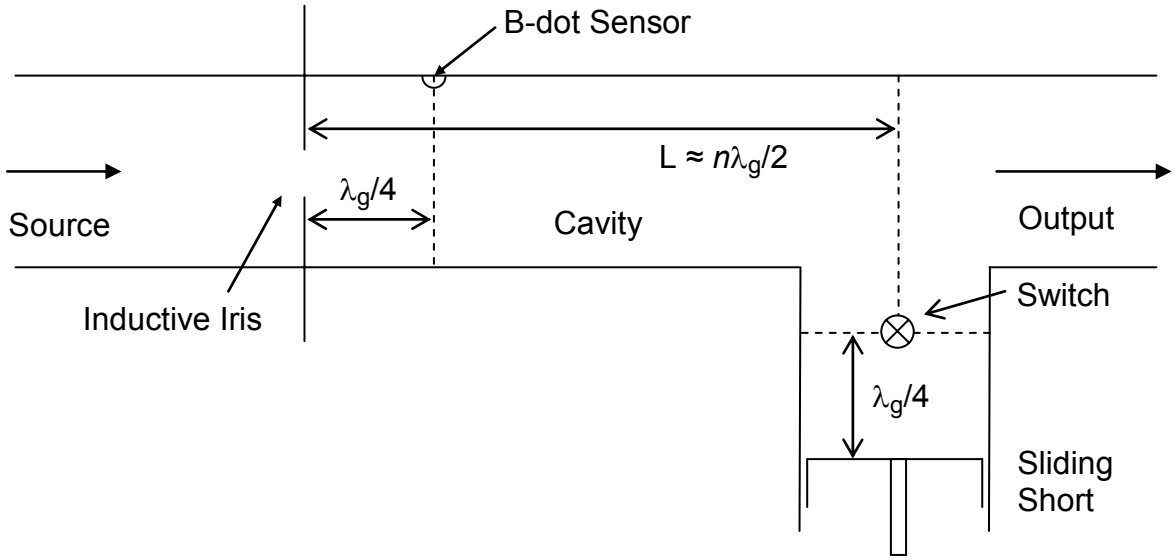

Figure 1. A sketch of Microwave Pulse Compressor, looking at the broad side of the waveguide.

.

The cavity has a length $L = (n\lambda_g)/2$, where λ_g is the guide wavelength,

$$\begin{aligned} \lambda_g &= \frac{c}{f\sqrt{1-(f_c/f)^2}} \\ f_c &= \frac{c}{2a} \end{aligned} \tag{1}$$

where f_c is the cutoff frequency of the waveguide, a is the waveguide width, and n is an integer. The output pulse width is expected to have a duration of one round-trip transit time at group velocity, or

$$\begin{aligned} T &= 2L/v_g \\ v_g &= c\sqrt{1-(f_c/f)^2} \end{aligned} \tag{2}$$

This suggests that long pulses require long cavities.

B. Relationship between Field and Power

Next, we establish a relationship between power and electric fields in the cavity, in order to estimate the electric fields that we have to tolerate. We consider a rectangular waveguide, in which a and b are the long and short cross-sectional dimensions, respectively. The dominant field of the TE_{10} mode is [10, eqn. 3.89b]

$$\begin{aligned} E_y &= \frac{-j\omega\mu_o a}{\pi} A_{10} \sin\left(\frac{\pi x}{a}\right) e^{-j\beta z} \\ \beta &= \sqrt{k^2 - (\pi/a)^2} = \frac{\omega}{c}\sqrt{1-(f_c/f)^2} \\ f_c &= \frac{c}{2a} \end{aligned} \tag{3}$$

where A_{10} is an arbitrary magnitude of the waveguide mode, and μ_o is the permeability of free space. So the square of the peak field in the center of the waveguide is

$$\left|E_y\right|^2 = \left(\frac{\omega\mu_o a}{\pi}\right)^2 \left|A_{10}\right|^2 \tag{4}$$

The power in a rectangular cavity TE_{10} mode is [10, eqn. 3.92]

$$P_{10} = \frac{\omega\mu_o a^3 b}{4\pi^2}\left|A_{10}\right|^2 \frac{\omega}{c}\sqrt{1-(f_c/f)^2} \tag{5}$$

for $f > f_c$. Taking the ratio of the last two equations, we find

$$\frac{\left|E_y\right|^2}{P_{10}} = \frac{4\eta}{ab\sqrt{1-(f_c/f)^2}} \tag{6}$$

where $\eta = \sqrt{\mu_o/\varepsilon_o} = \mu_o c = 377\ \Omega$. This can be recast as

$$\left|E_y\right| = 2\sqrt{\frac{\eta P_{10}}{ab\sqrt{1-(f_c/f)^2}}} \tag{7}$$

Finally, voltage is just the field times the waveguide height, since the field is constant in the vertical direction, or

$$V = b\left|E_y\right| = 2\sqrt{\frac{b}{a}\frac{\eta P_{10}}{\sqrt{1-(f_c/f)^2}}} \tag{8}$$

For WR-650 waveguide, a = 16.51 cm, b = 8.255 cm, b/a = 0.5, and f_c = 0.91 GHz. Thus, at our operating frequency of f = 1.3 GHz, we have $\sqrt{1-(f_c/f)^2} = 0.72$. Under these assumptions,

$$V \approx 32\ (\Omega)^{1/2}\sqrt{P_{10}} \tag{9}$$

We can tabulate this data for a number of input powers, ranging from a 100-Watt amplifier to a 3 MW amplifier used at high power. We assume that the cavity is well matched, and that the gain in the cavity is 20 dB.

Table 1. Cavity electric field and voltage versus input power, assuming 20 dB cavity gain.

P_{in}	P_{cavity}	V (kV)	$\|E_y\|$ (kV/cm)
100 W	10 kW	3.2	0.39
1 kW	100 kW	10	1.2
10 kW	1 MW	32	3.9
100 kW	10 MW	100	12
1 MW	100 MW	320	39
3 MW	300 MW	550	67

Note that with 3 MW of input power, the cavity electric field is already well above the 30 kV/cm threshold for flashover in air at sea level. This suggests that SF_6 will be required in the high-power experiments.

C. Some Experimental Details

We experimented with an iris with a variable width to estimate the optimal opening. A conceptual drawing of this is shown in Figure 2. We found experimentally that we obtained the largest cavity field with a opening of $w = a/4$, so we used that value consistently throughout our measurements.

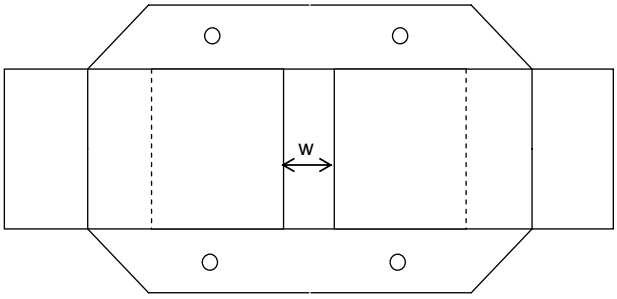

Figure 2. Inductive iris with variable width.

To tune the cavity, we first had to estimate the cavity length. We found the following estimate experimentally,

$$L \approx n \lambda_g / 2 - 0.1 b \tag{10}$$

where b is the long dimension of the cross section of the waveguide that forms the cavity and tee. In practice, this was a little longer than required, so we had to mill off a small portion of a waveguide flange or spacer, to find a resonance at the desired frequency. Of course, the sliding short always had to be adjusted carefully to provide the maximum field within the cavity, as measured by a Vector Network Analyzer.

We converted oscilloscope readings to power levels as follows. First, we dialed into each channel of our oscilloscope the attenuations for each channel, which included calibration factors for each sensor. Next, we averaged the envelope of the voltage measurement near the peak. Finally, we converted the voltage to average power using the formula

$$P_{avg} = \frac{V_{peak}^2}{2 \times 50\ \Omega} \tag{11}$$

where V_{peak} is the local average of the peak voltage envelope.

All sensor calibration factors were measured with a Vector Network Analyzer (VNA). To do so, we inserted the sensor or directional coupler between lengths of WR-650 waveguide, with waveguide to coax adapters at either end, and with all unused ports terminated in 50 Ω. In this configuration, S_{21} is the calibration factor of the sensor.

III. Low-Power Measurements

We provide here the results of our pulse compression experiments at 1.3 GHz, in WR-650 rectangular waveguide, driven by a 1 kW amplifier.

We experimented with a variety of switches, including triggered and untriggered gas discharge tubes (GDTs) filled with low-pressure air. We found that if we controlled the pressure carefully, the switch would self-break, however its reliability was poor. To address this, we added a trigatron to ensure that the switch fired consistently when the cavity approached a maximum stored energy. Typical operating pressures were around 10-13 mTorr, which were on the left side of the Paschen curve for breakdown of air.

A. Experimental Configuration

The experimental configuration is shown in Figure 3. The resonant cavity was a length of WR-650 rectangular waveguide, either $3\lambda_g$ or $5\lambda_g$ in length, where λ_g is the guide wavelength. The cavity was constrained on the input end by an inductive iris centered in the waveguide, with a slot width of one-quarter the waveguide width. On the output end, the cavity was constrained by an H-plane tee, with a sliding short tuned to provide an optimal resonance. The gas discharge tube (GDT) containing the switch was positioned $\lambda_g/4$ from the sliding short.

The input signal was 1 kW, the pulse repetition frequency was 10 Hz, and the input pulse width was 1.5 μs. The switch consisted of a Gas Discharge Tube (GDT) of low-pressure dried air. The GDT was fabricated from a polyethylene tube, with 3/8 in. outer diameter, 1/4 in. inner diameter, and smooth copper electrodes at either end, with 1/4-in. outer diameter. The end cap of one of the electrodes had two small holes that allowed one to apply a vacuum.

Pulsed CW was emitted from the amplifier with pulse repetition frequency of 10-50 Hz, and pulse width of 1.5 μs, at a frequency of 1.3 GHz. The delay pulser, the SRS model DG535, controlled the frequency and pulse width of the pulsed CW driving the cavity. It also controlled the timing of the trigatron pulser.

To stabilize the switch timing, we added a trigatron to our switch. Thus, at one end of our Gas Discharge Tube (GDT), we placed a spark gap that was triggered by a Grant Applied Physics model HYPS source, with 4 kV peak voltage and 3 ns pulse width. Photos of the trigatron are shown in Figure 4. We flowed the gas in the switch, and we dried the air with a desiccating agent.

Data were recorded from directional couplers positioned at the input and output to the cavity. Data were also recorded from a small loop (B-dot) sensor positioned in the side wall of the cavity, positioned to record the maximum value. All data channels were calibrated to show voltages on consistent vertical scales. Data were recorded on a Tektronix model TDS6804 oscilloscope, at a resolution of 0.1 ns/point, or 10 gigasamples/second.

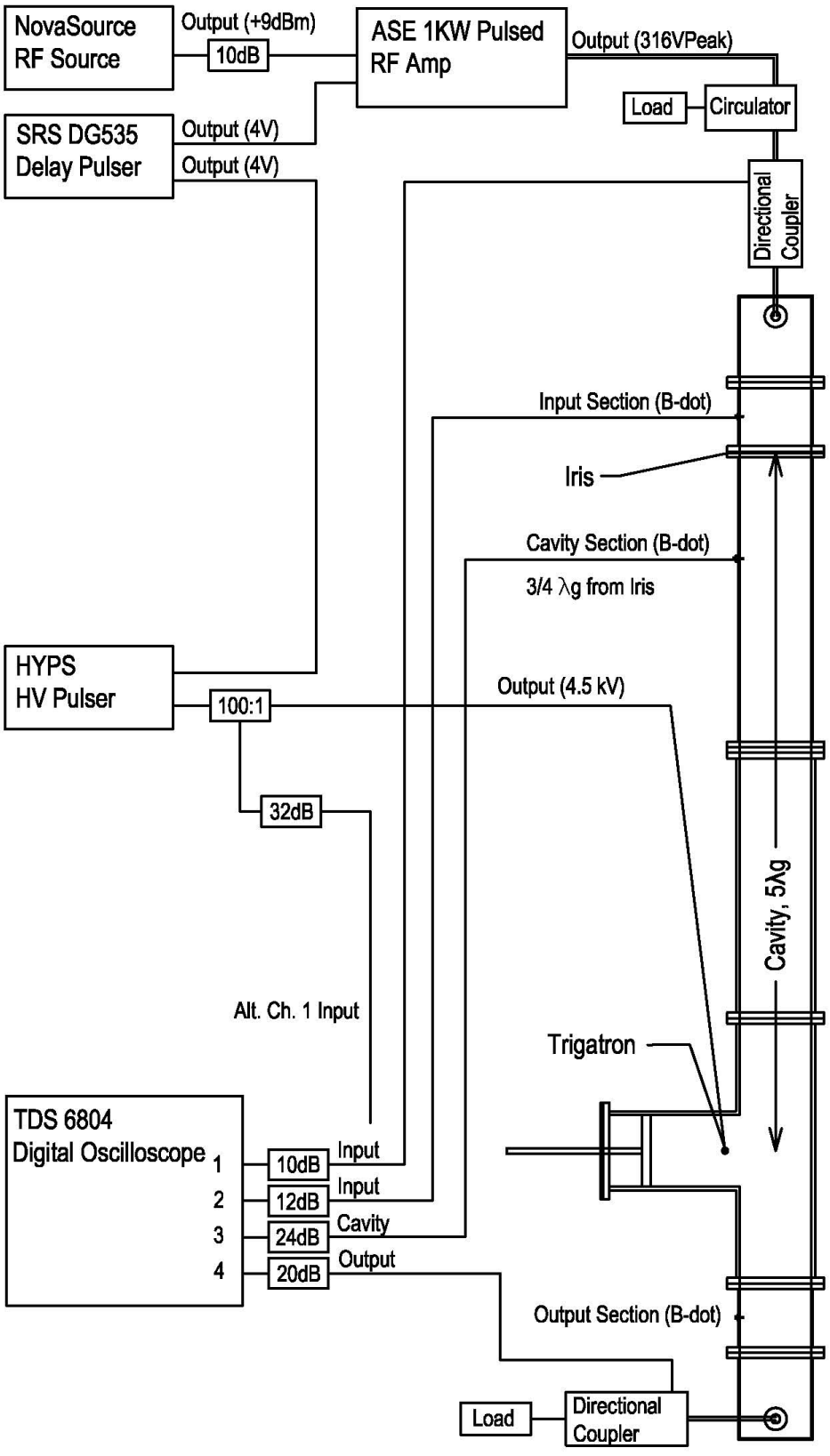

Figure 3. Experimental setup of microwave pulse compression.

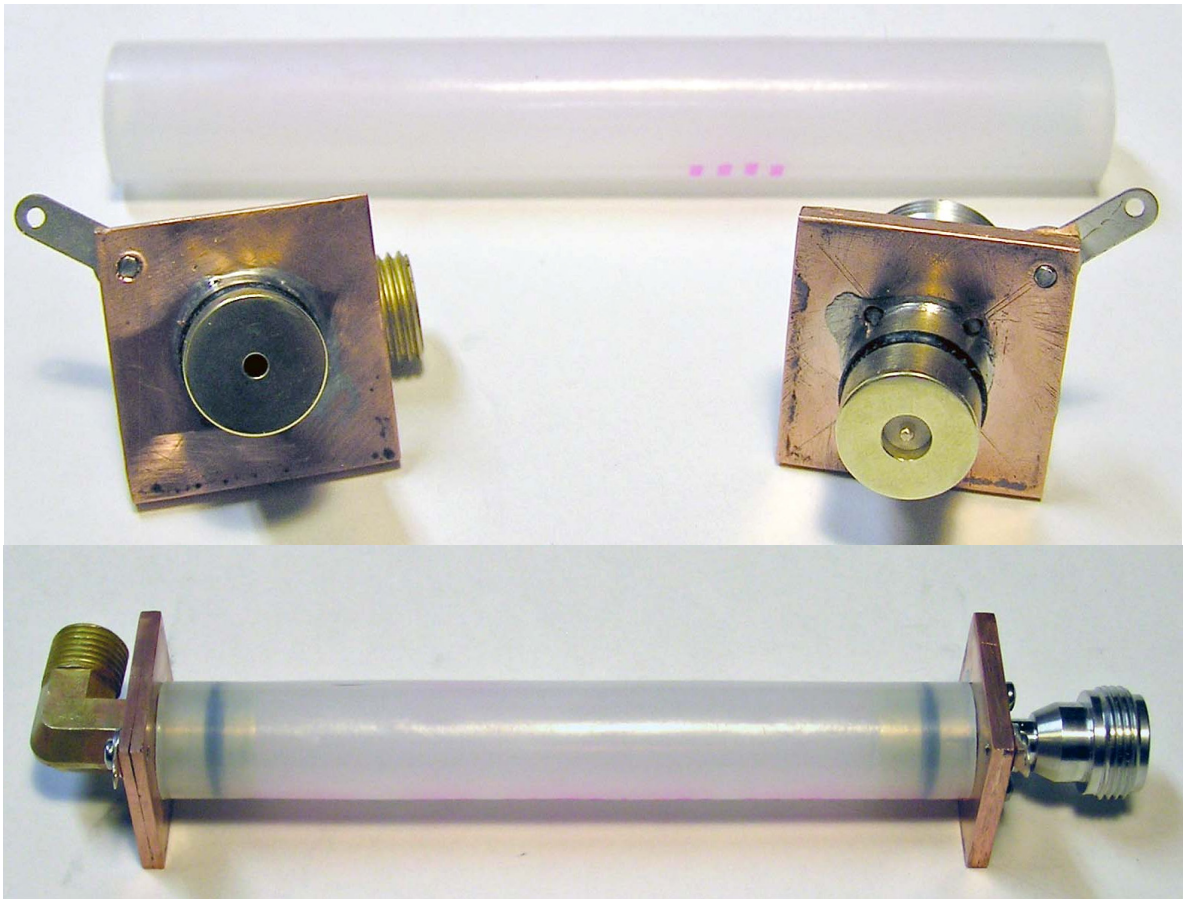

Figure 4. Details of the trigatron and Gas Discharge Tube Switch. .

B. Results

We recorded three channels of output, as shown in Figure 5; the directional coupler at the input section (top), the small loop (B-dot) sensor in the cavity (middle), and the directional coupler in the output section (bottom). From this, we see clearly that the switch fires at the proper time, when the cavity is nearly full. Note that the vertical scales have been compensated for attenuators and sensor calibration factors. In this case, with a trigatron, we observed a gain of around 11.6 dB from the input to the output. In the next section, we reach 15.6 dB gain by operating in self-break mode. And in Section III.E, we reach 13.6 dB of gain, using a trigatron driven by an FID pulser in a 10 λ_g cavity.

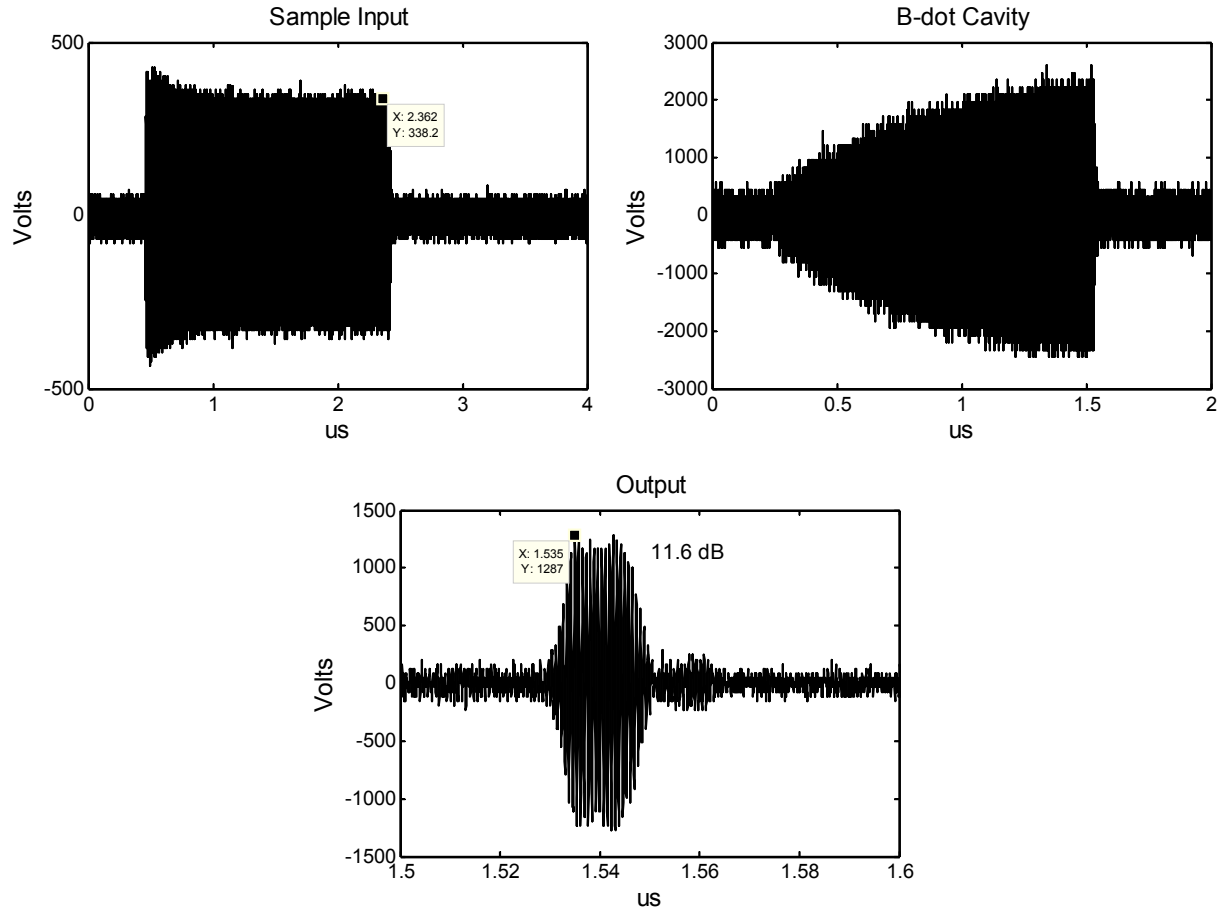

Figure 5. The signals from the input waveguide (top left), cavity (top right), and output (bottom). Note that all three vertical scales are consistent, because attenuators and sensor calibration factors have been entered into the oscilloscope.

C. Pulse Width and Risetime/Falltime

We compared the length of an output pulse in a cavity that is 3 λ_g and 5 λ_g in length. The results are shown in Figure 6, where we observe that the 3 λ_g cavity produces an output 9 ns in length, and the 5 λ_g cavity produces an output 15 ns in length, measured at Full-Width Half Maximum (FWHM). We compared these pulse widths to those expected by the round-trip transit time at group velocity, and found good agreement in both cases.

Note that the data taken in Figure 6 were taken without a trigatron, and in this series of measurements we obtained slightly better gain. The data here can be compared to the input signal in Figure 5, so we see that we have 15.2 dB of gain with the 3 λ_g cavity.

Next, we estimated the risetime and falltime of the data in Figure 6 (left), by simply expanding the scales, as shown in Figure 7. We estimate a risetime of 2.5 ns and fall time of 4 ns.

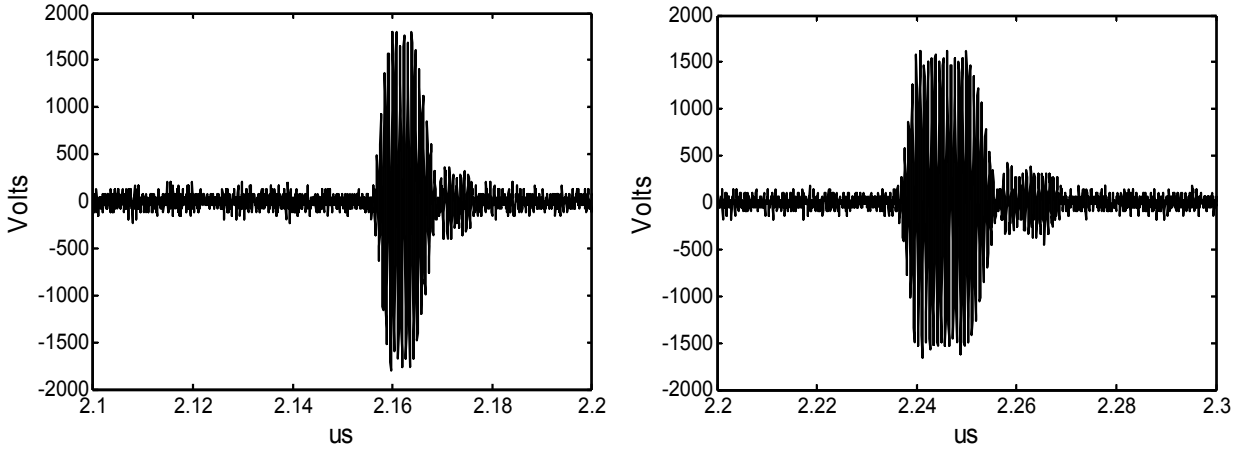

Figure 6. Pulse width study for a 3 λ_g cavity (left) and 5 λ_g cavity (right).

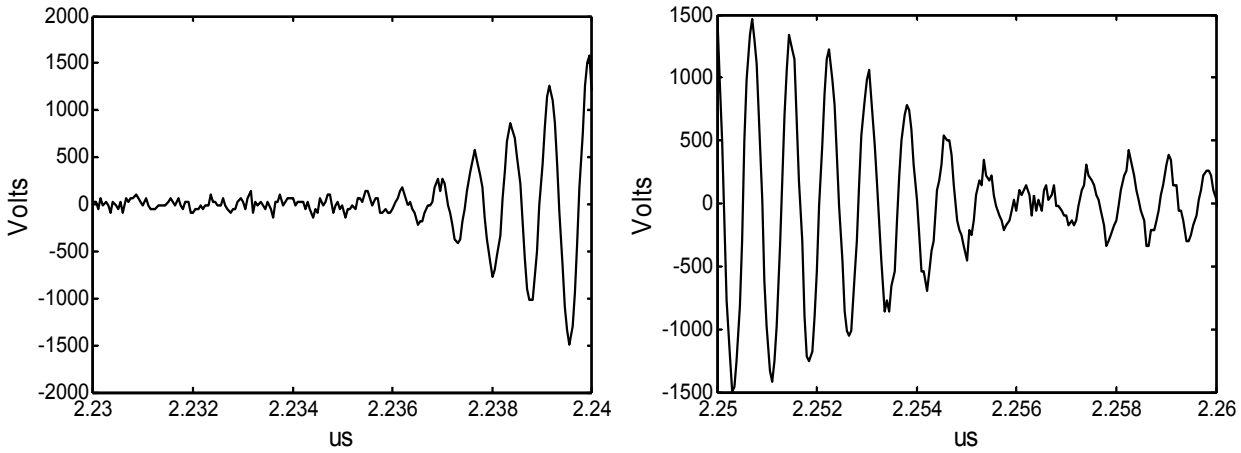

Figure 7. Risetime and fall time of the data in Figure 6 (left).

D. Gain Study

We explore here the best possible theoretical cavity gain that can be realized with our pulse compression configuration. In [11], Andreev *et al* consider the simplest possible type of cavity – a shorted cavity of length (n λ_g)/2, with an inductive iris aperture, as shown in Figure 8. Note that our configuration does not have a short circuit, but an H-plane tee with a sliding short. So this theory provides a best case calculation.

With an optimal iris opening, the optimal gain within the cavity is

$$G_{opt} = \frac{1}{4\alpha L} \tag{12}$$

where L is the length of the cavity waveguide in meters, and α is the attenuation of the waveguide in Np/meter. We find the midband attenuation constant of WR-650 waveguide is 0.25 dB/100 ft, or 0.008 dB/m. Noting that 1 Np = 8.68 dB, we find $\alpha \approx 0.001$ Np/m. Thus, for a 3 λ_g cavity, we find G_{opt} = 24 dB. We observed 22 dB in our cavity, so we are close to the theoretical maximum.

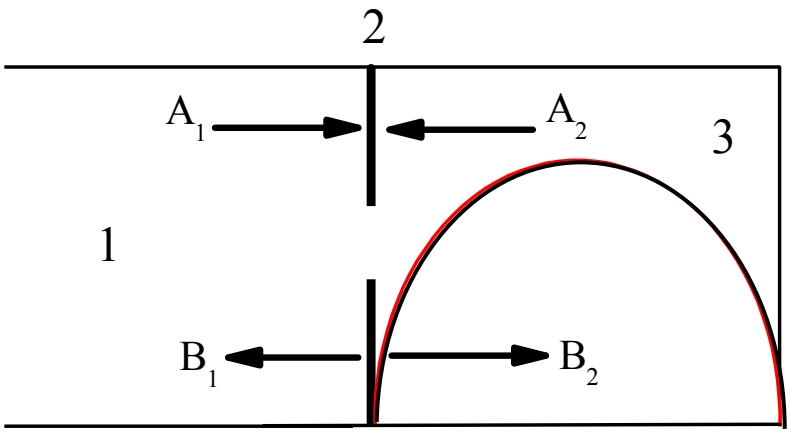

Figure 8. The configuration analyzed in Andreev *et al*..

E. Network Analysis

We measured the steady-state CW return loss of the cavity, and the cavity gain, relative to a calibrated measurement in a waveguide without the cavity. This data was taken with an Agilent model 8753ES Vector Network Analyzer. The results are shown in Figure 9, where we see that the return loss at resonance is better than –12 dB, and the cavity gain at resonance is 19 dB.

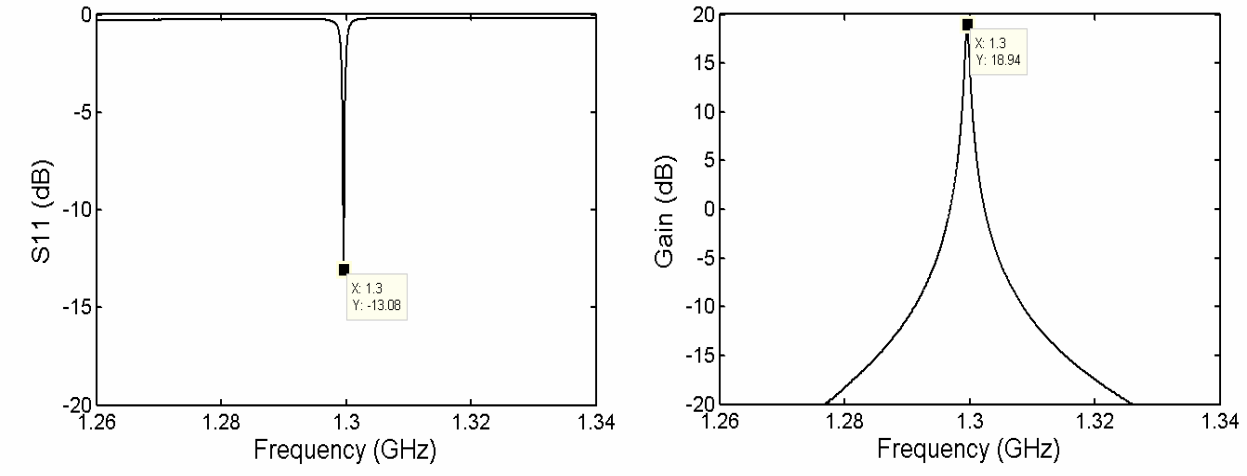

Figure 9. Steady-state CW S_{11} of the input to the cavity (top) and cavity gain (bottom).

F. Low-Power Simulation of High-Power Experiments

We carried out a series of low-power experiments as a direct simulation of the planned high-power experiments. Thus, we replaced the HYPS trigger pulser used earlier with an FID pulser, of peak voltage 20 kV and pulse width of 3 ns. We lengthened the cavity to 10 λ_g, and we sealed the flanges with RTV (room temperature vulcanizer, a silicon sealant), which was later replaced with gaskets during the high power measurements. The experimental test configuration is shown in Figures 10 and 11. A trigatron with gas discharge tube was used, with dried air at a pressure of 1.2 Torr. The source pulse width was 2.2 μs, and the repetition rate was 10 Hz,

Data for this configuration is shown in Figure 12. We realized 22 dB of gain within the cavity, and 13.6 dB of gain at the output.

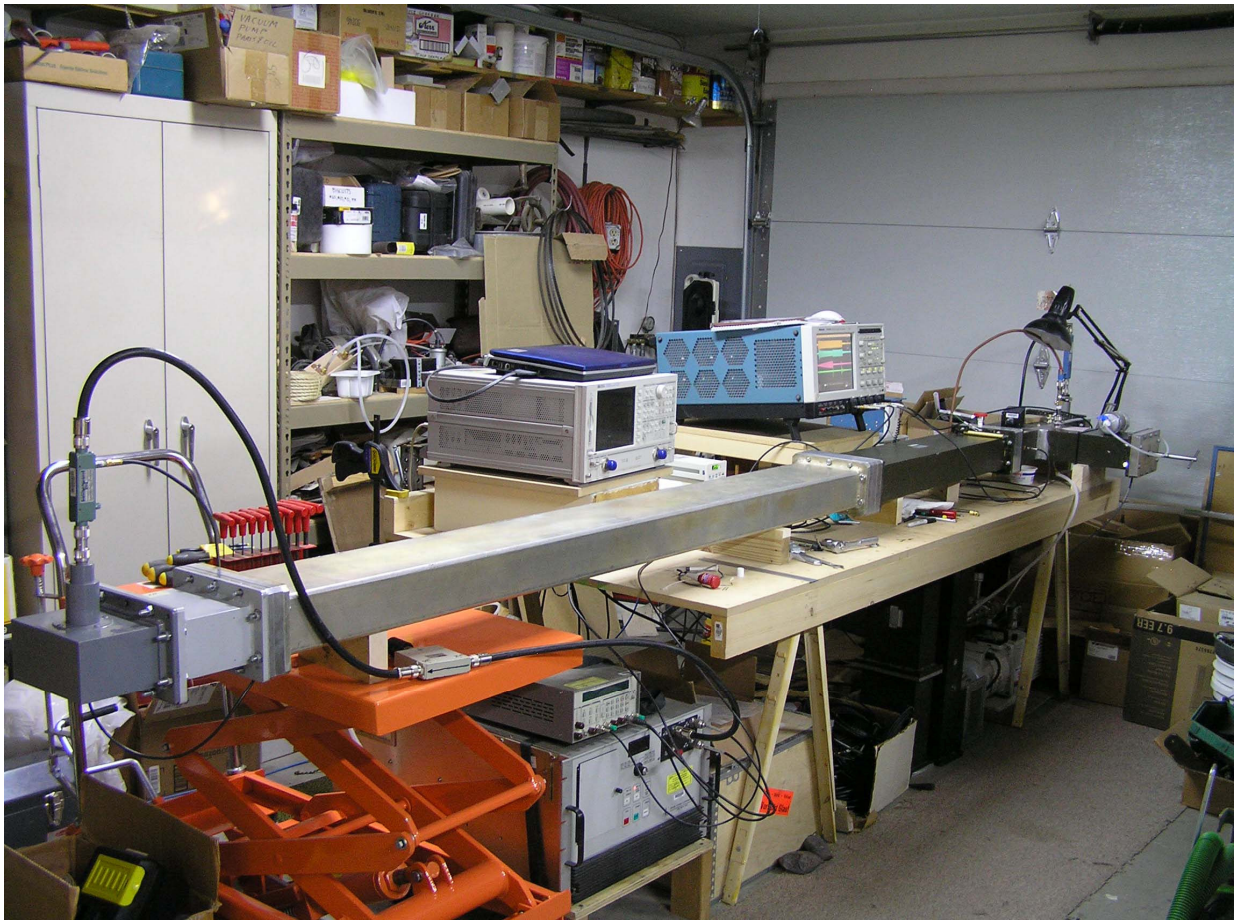

Figure 10. Photo of the low-power simulation of high-power experiments.

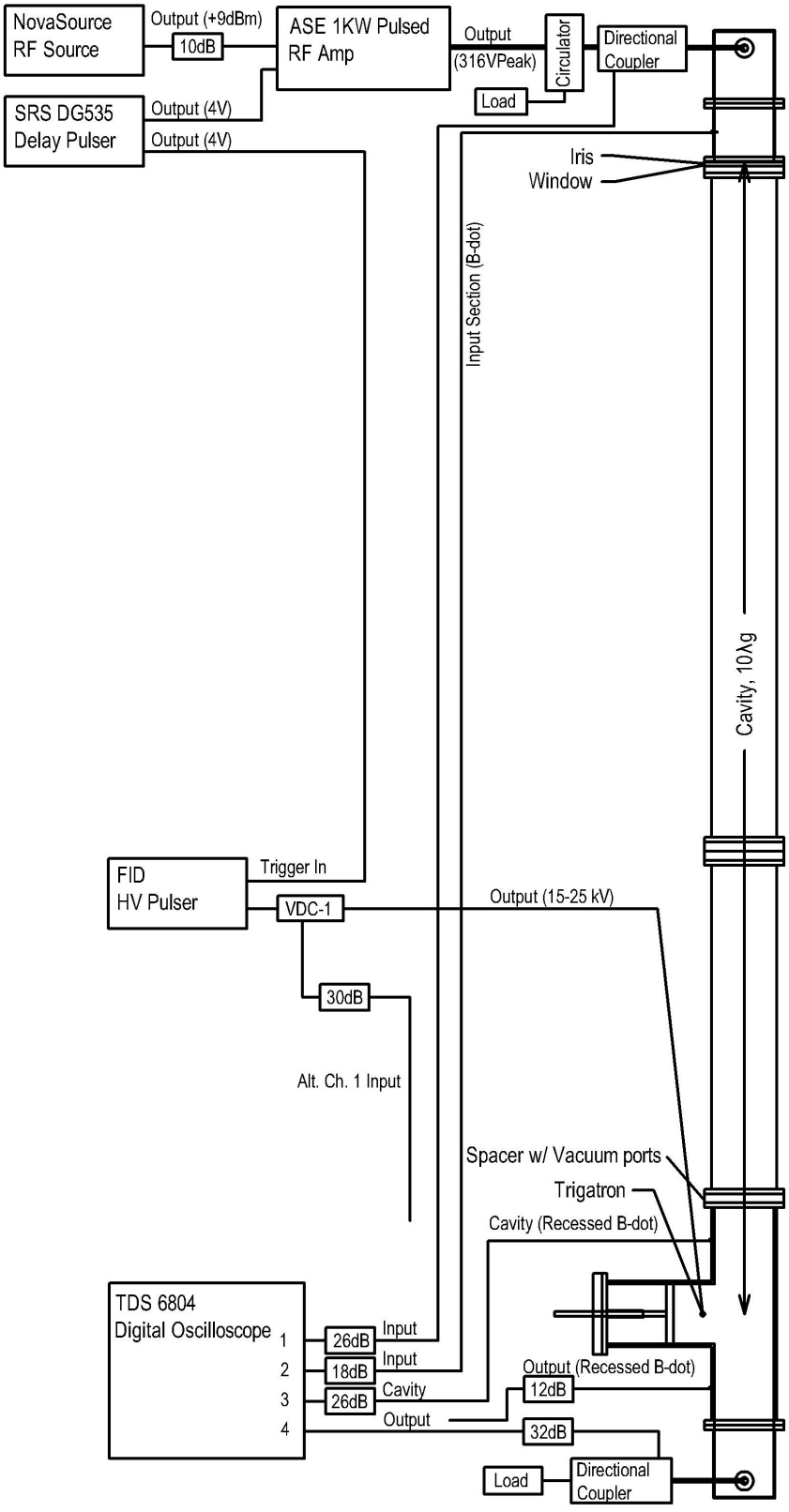

Figure 11. Experimental setup of the low-power simulation of high-power experiments.

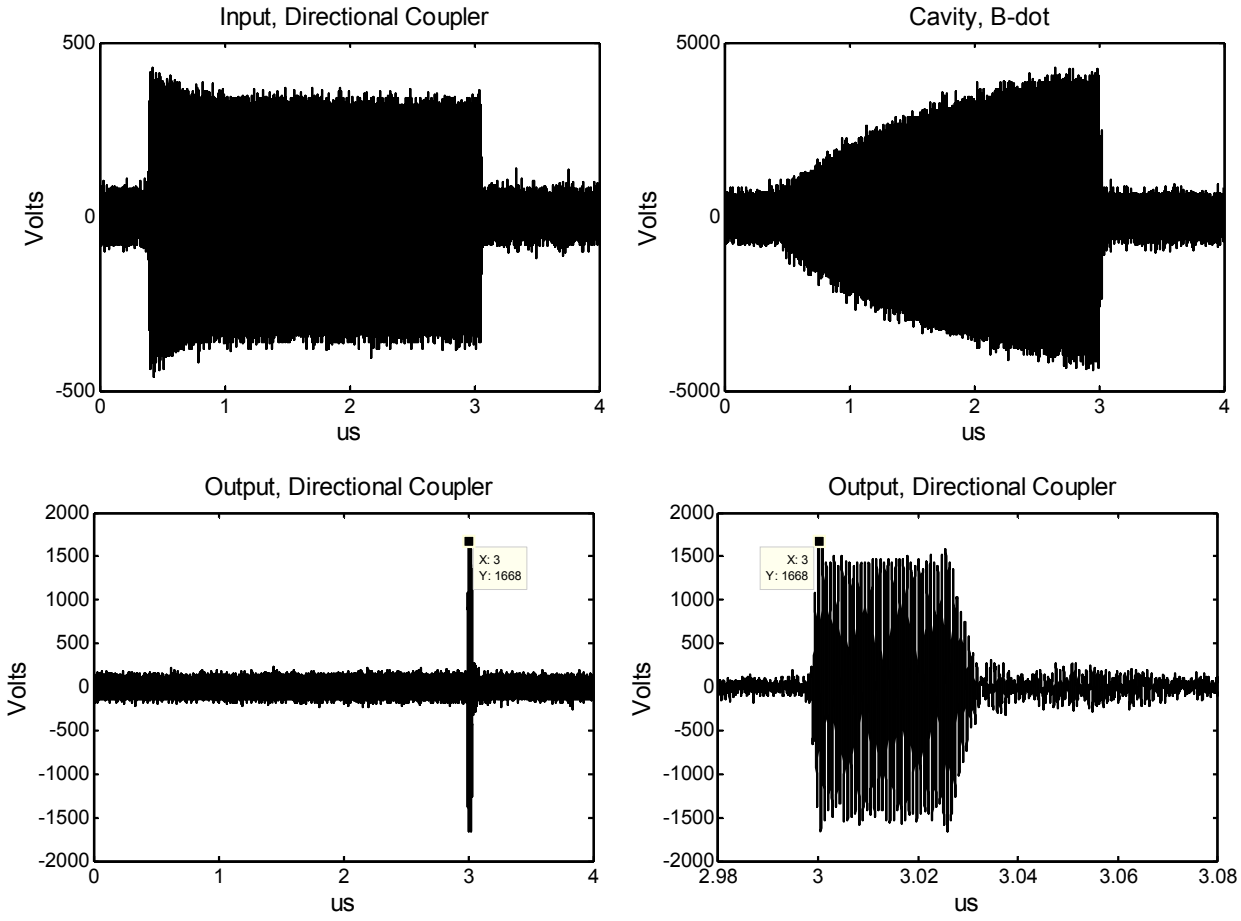

Figure 12. Data from the low-power simulation of the high-power experimetns.

IV. High Power Measurements

Next we describe the setup of our high-power measurements, as shown in Figures 13 – 16.

We used the FRED source (Frequency Radio Engine Disruptor), owned by AFRL, to drive the cavity at 2.8 MW, with pulse repetition frequencies ranging over 5 Hz to 160 Hz. This source was actually capable of 5-6 MW, with peak PRF of 400 Hz.

After the FRED source, we placed a high-power 4-port circulator, to protect the source. The two unused ports were terminated with either a high-power or a low power load. Next, at the input to the cavity, we placed an inductive iris with a ribbed window made of polycarbonate (Lexan), as shown in Figure 17. The cavity was about 3.26 meters in length, from the aperture to the center of the H-plane tee, which corresponded to 10 λ_g at 1.3 GHz. In the H-plane tee was a sliding short for tuning, shown in Figure 18, and a trigatron with a 1 mm gap, as shown in Figures 19 – 20. This was driven by a 20 kV FID pulser with a pulse width of 3 ns FWHM. After the tee was a high-power load manufactured by Voss Scientific. The cavity, tee, sliding short, and load were all sealed in order to maintain a pressure of 20 psig SF_6.

We detected the signal at three points in the configuration; a directional coupler at the output of the FRED source, a B-dot (loop) sensor in the cavity, and a directional coupler at the output. To prevent flashover, the B-dot sensor was recessed into the thick wall of the cavity. A photo of the B-dot sensor is shown in Figure 21. It was calibrated with a Vector Network Analyzer (Agilent model 8720ES) in a straight section of waveguide with two waveguide-to-coax adapters. We also detected the output of the FID pulser using a V-dot cable sensor, a Farr Research model VDC-1.

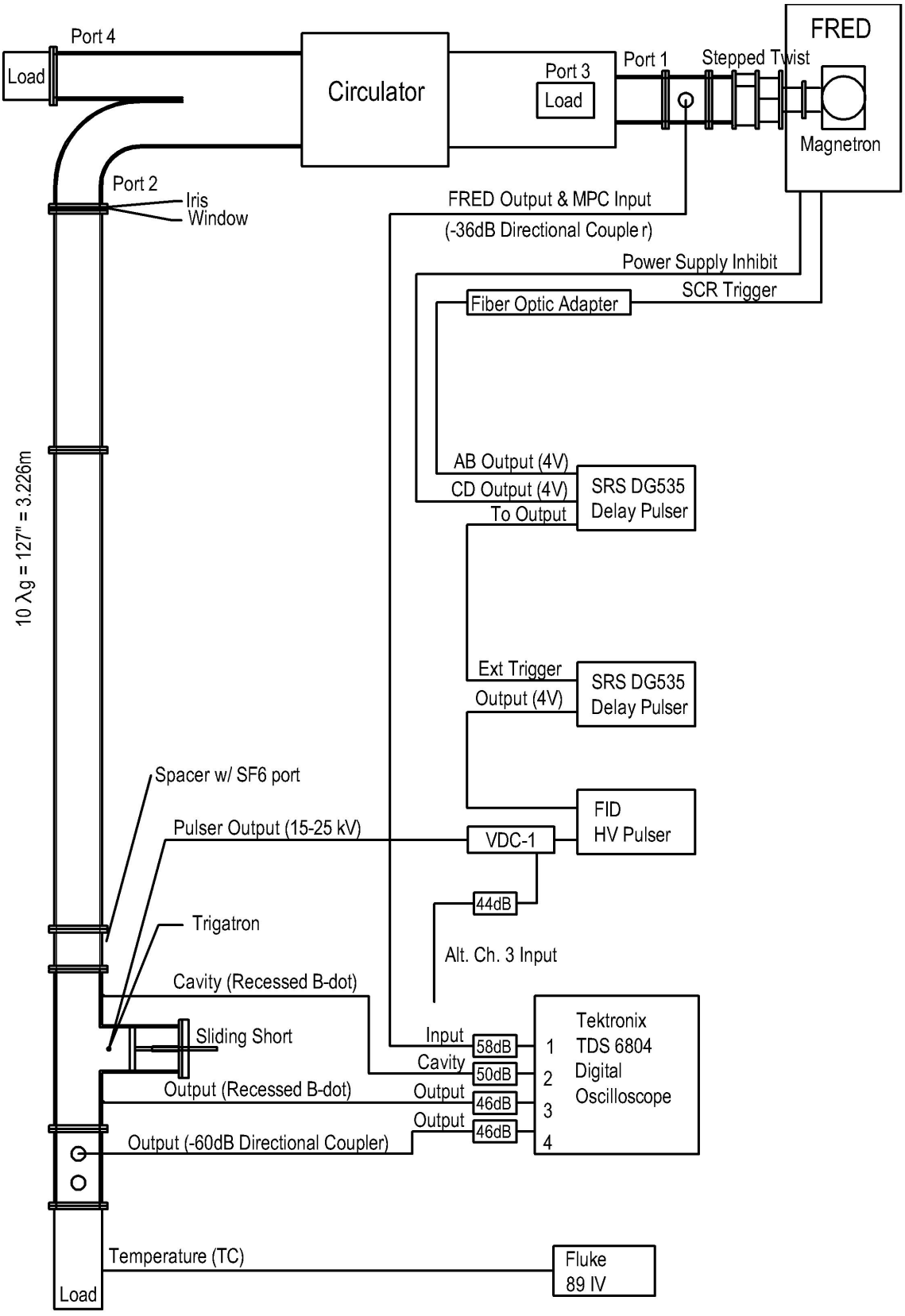

Figure 13. Experimental setup for high-power MPC measurements.

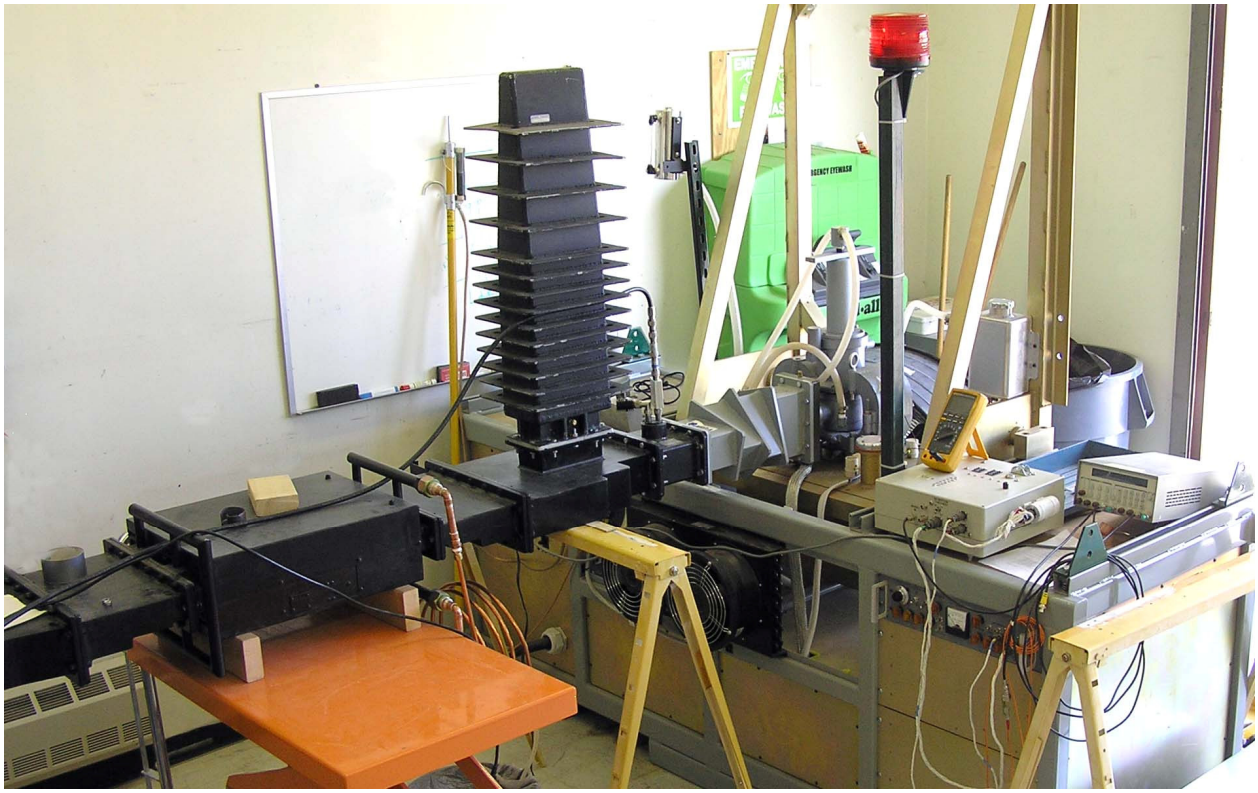

Figure 14. Photo of the FRED source and ciruclator.

Figure 15. Photo of the cirulator and cavity.

Figure 16. Photo of the cavity, H-plane tee, sliding short, and load.

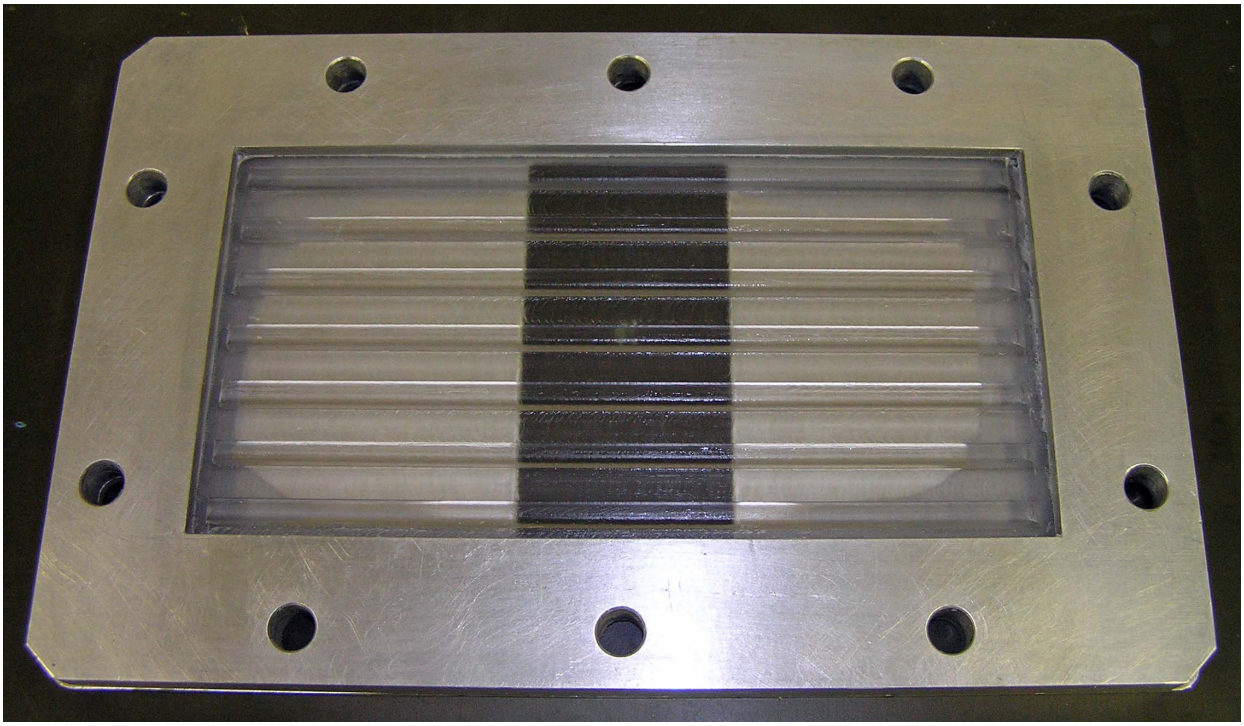

Figure 17. Photo of the inductive iris and ribbed window.

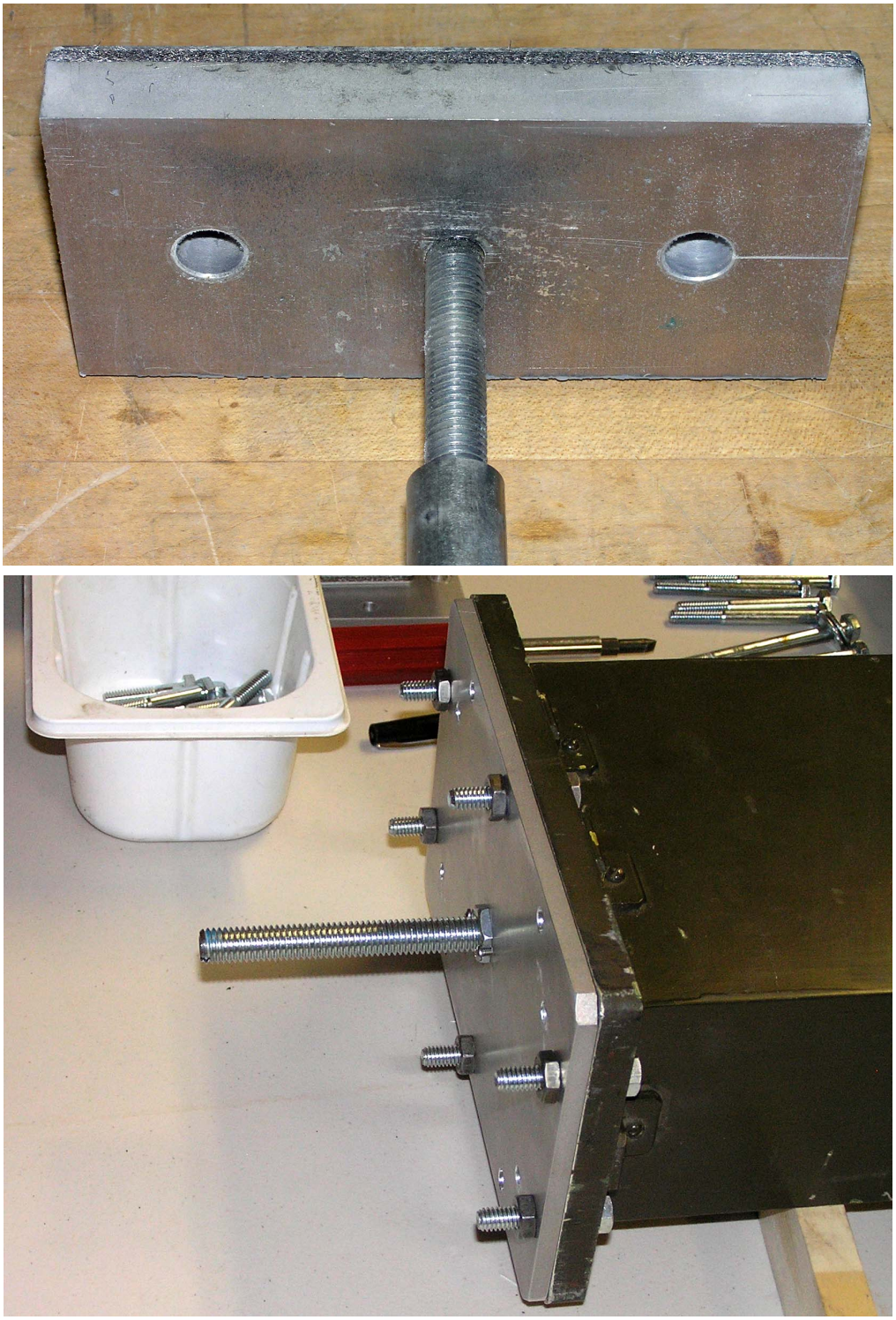

Figure 18. Two views of the sliding short, the plunger (top) and the exterior (bottom).

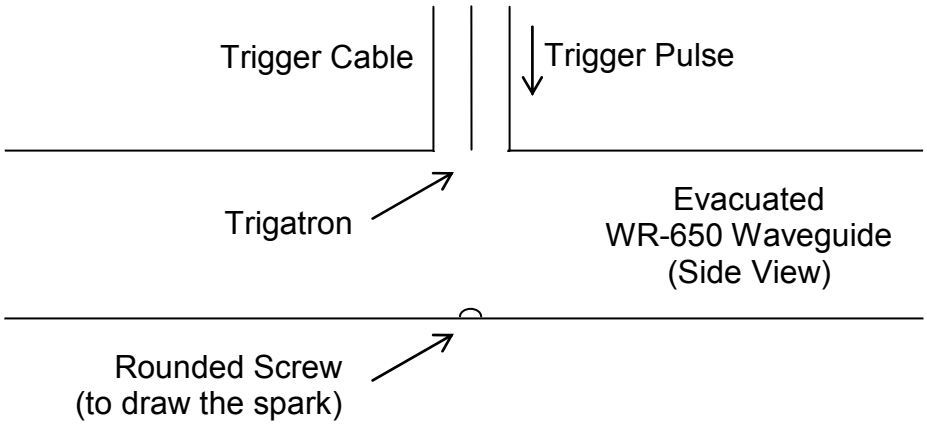

Figure 19. Trigatron concept.

Figure 20. Photo of the trigatron.

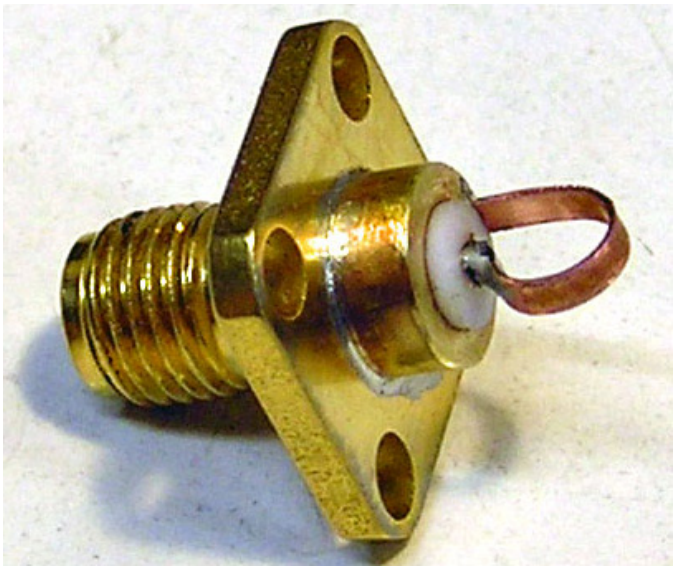

Figure 21. Photo of B-dot sensor.

All data were recorded on a Tektronix model TDS6804. real time oscilloscope, with 8 GHz of realtime bandwidth, and with a Δt of 50 ps, which provided a sampling range of about 15 samples per cycle at 1.3 GHz.

Data from a typical shot is shown in Figures 22-23. This particular data set was taken at a Pulse Repetition Frequency (PRF) of 100 Hz, although the MPC worked over a range of 5-160 Hz. We drove the cavity with a microwave pulse of 2.8 MW input and realized 330 MW in the cavity and 51.8 MW at the output. This corresponded to gains of 20.7 dB in the cavity, and 12.7 dB in output. The operating frequency for this shot was 1.2982 GHz. In the cavity data, one can see the power build up until a peak is reached, and then is suddenly reduced when the trigatron is fired.

To calculate the peak power levels, we first calculated the envelope, and took the average through the envelope over a short range of time at the peak of the waveform. This process was more accurate than simply taking the absolute peak of the waveform, which could be high by as much as 3 dB. The process is diagrammed on the right side of Figure 23.

We calculated the efficiency as follows. The input source was 2.8 MW and charged the cavity for 3.4 μs, and their product is an energy of 9.5 J. The output pulse was 51.8 MW for 45 ns (FWHM), and their product is an energy of 2.3 J. The ratio of the energies is 24%, which is the efficiency of the pulse compressor.

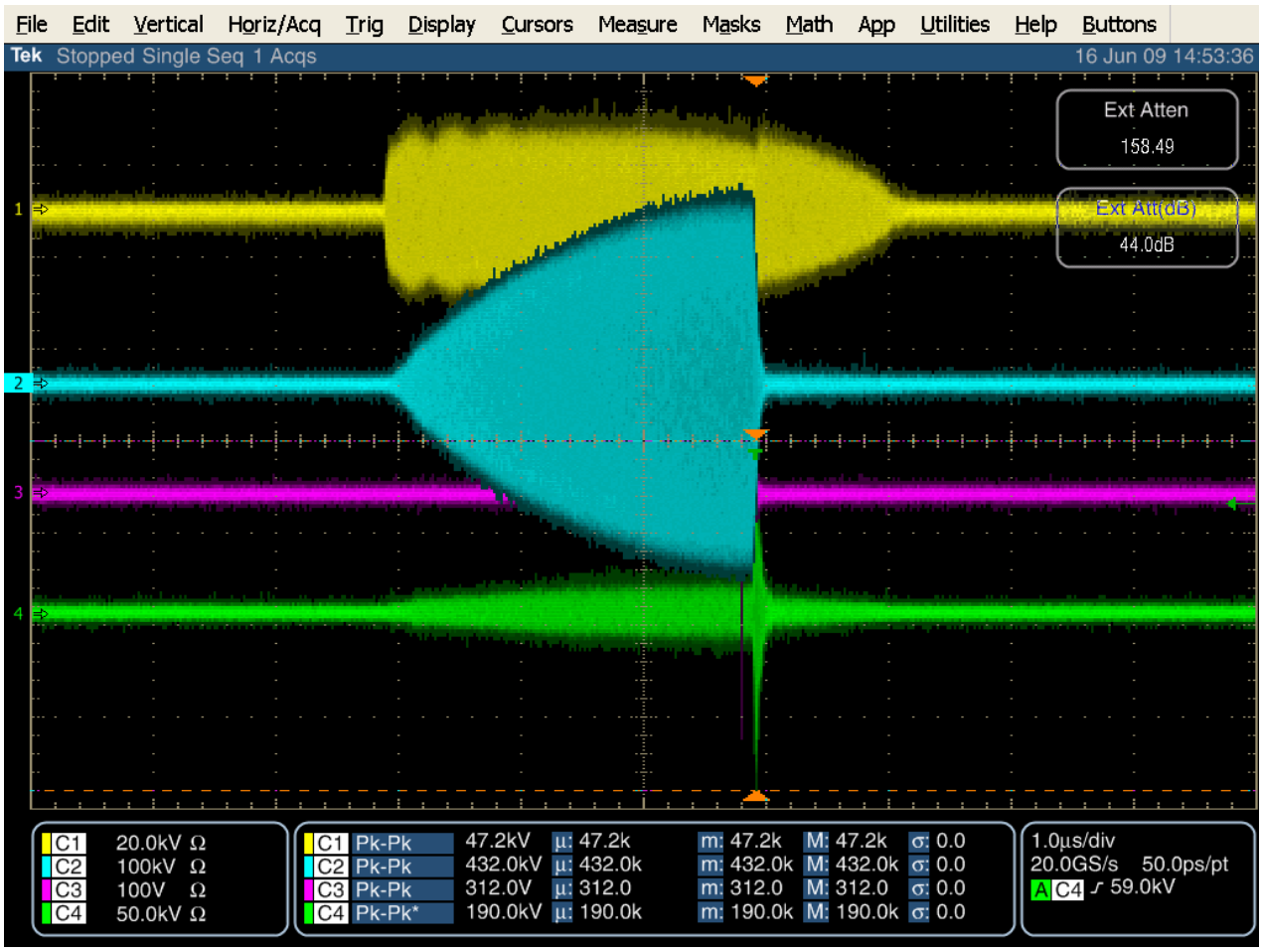

Figure 22. Oscilloscope traces of the data, from top to bottom, Input, Cavity, Trigger Line, and Output. All scales are adjusted for attenuators and sensor calibration factors.

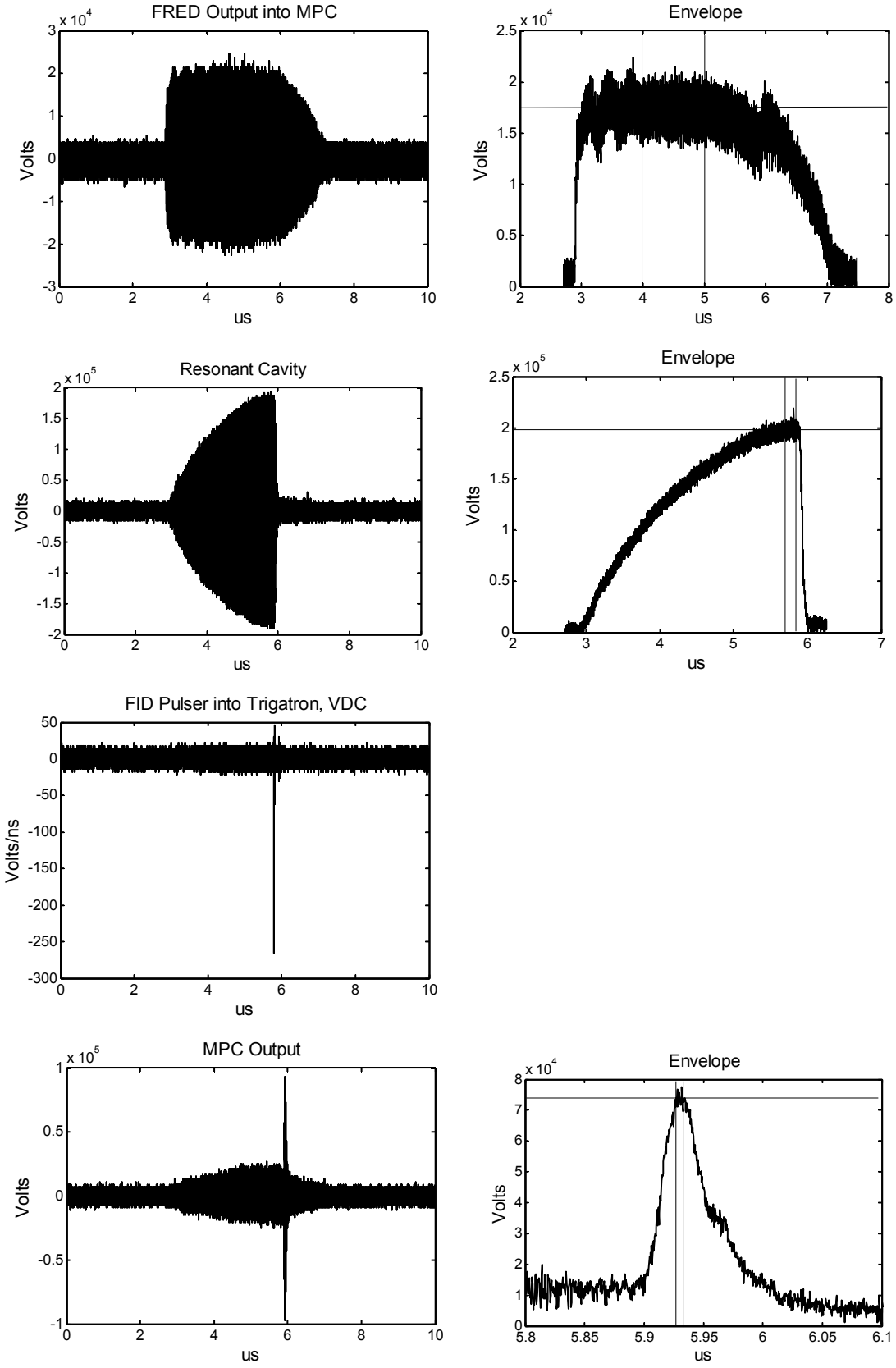

Figure 23. Oscilloscope trace data , left, and the corresponding envelope, right.

Next, we provide typical VNA data for our cavity, in Figure 24. On the left is the return loss, S_{21}, and on the right is the coupling into the cavity, as measured with an uncalibrated B-dot sensor. Based on the return loss, we observe that we have a very narrow frequency window within which we can operate. The return loss has a –3 dB bandwidth of 360 kHz, which leads to a Q of $f_o/\Delta f$ = 1.3 GHz / 360 kHz or 3600.

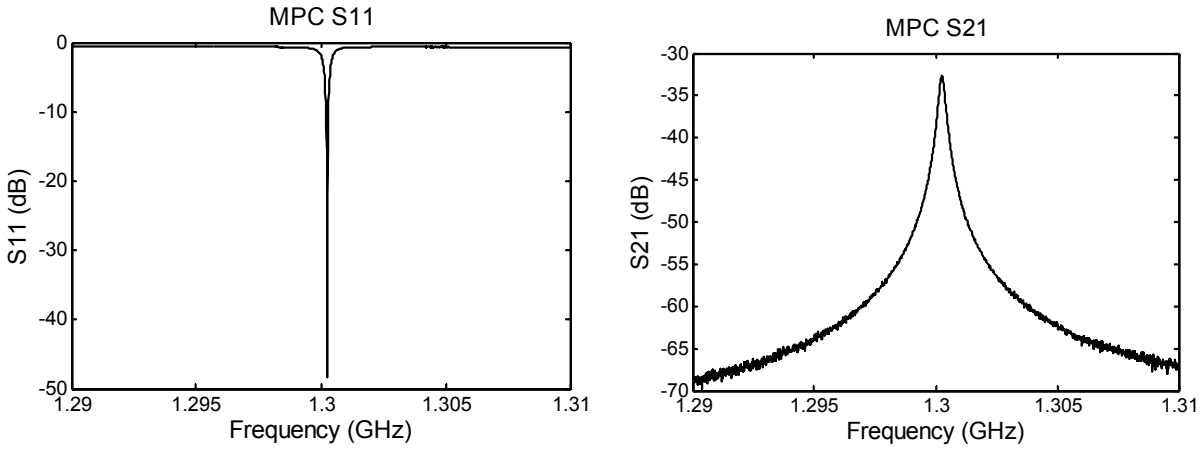

Figure 24. Sample network analyzer data, S_{11} (left) and S_{21} (right). Note that the scale on the S_{21} data is arbitrary, since the response of the B-dot probe was not taken into account.

Finally, we note that we initially thought a Gas Discharge Tube (GDT) would be necessary at high power, as it was at low power. So we built a tube with a scalloped exterior, as shown in Figure 25. But we observed premature arcing along the interior surface of the tube, before full power was reached within the cavity. We wanted to scallop the interior of the tube, but that was difficult to realize mechanically. The solution was to use a simple trigatron without a GDT.

Figure 25. Gas Discharge Tube for high power experiments.

V. Discussion and Future Work

We consider here the limitations of the technique, and how it could be developed further. We then consider possible future work.

The FRED source we used was capable of 5-6 MW output, however we only used 2.8 MW in our experiments. We were limited primarily by premature breakdown in the cavity, which reached a power level of around 360 MW in 20 psig SF_6. To reduce flashover, we would need to use a smoother cavity, and place flanges precisely at nulls in the resonance pattern. We assembled our cavity from available parts, and we made many improvements where we could, but it would have been better to start with fresh waveguide that was built to high tolerance, with precisely aligned flanges and alignment pins.

We could also obtain higher power with a higher pressure of SF_6. We were reluctant to use a pressure higher than 20 psig because of the slow leakage of expensive gas from our flanges and directional couplers. We used gaskets at all flanges, but one of the directional couplers appeared to have a small leak through a connector. If we started with components that were specifically designed for pressure, we could have realized a higher pressure, and higher output.

We see three areas where future work would be beneficial. First, by sealing leaks and using smoother components, we should be able to realize higher power. Second, FRED source is a somewhat large and cumbersome source, that was not tailored to our specific need. It should be possible to design a more compact microwave driver that is less massive.

Finally, it would be of interest to design a tunable cavity, since vulnerability testing normally requires exposure to a range of frequencies. We are limited by the tunability of the available sources, but tunable sources seem to be available over a limited bandwidth. Two concepts for tunable MPCs are sketched in Figure 26. A magic tee is used to split the signal into two identical cavities, whose lengths are controlled by sliding shorts that are tuned in tandem. Because of symmetry, no signal leaves the output port until symmetry is broken by firing a switch in one of the cavities. On the bottom of Figure 26, we show how the two sliding shorts could be combined into a single unit, to simplify the mechanics.

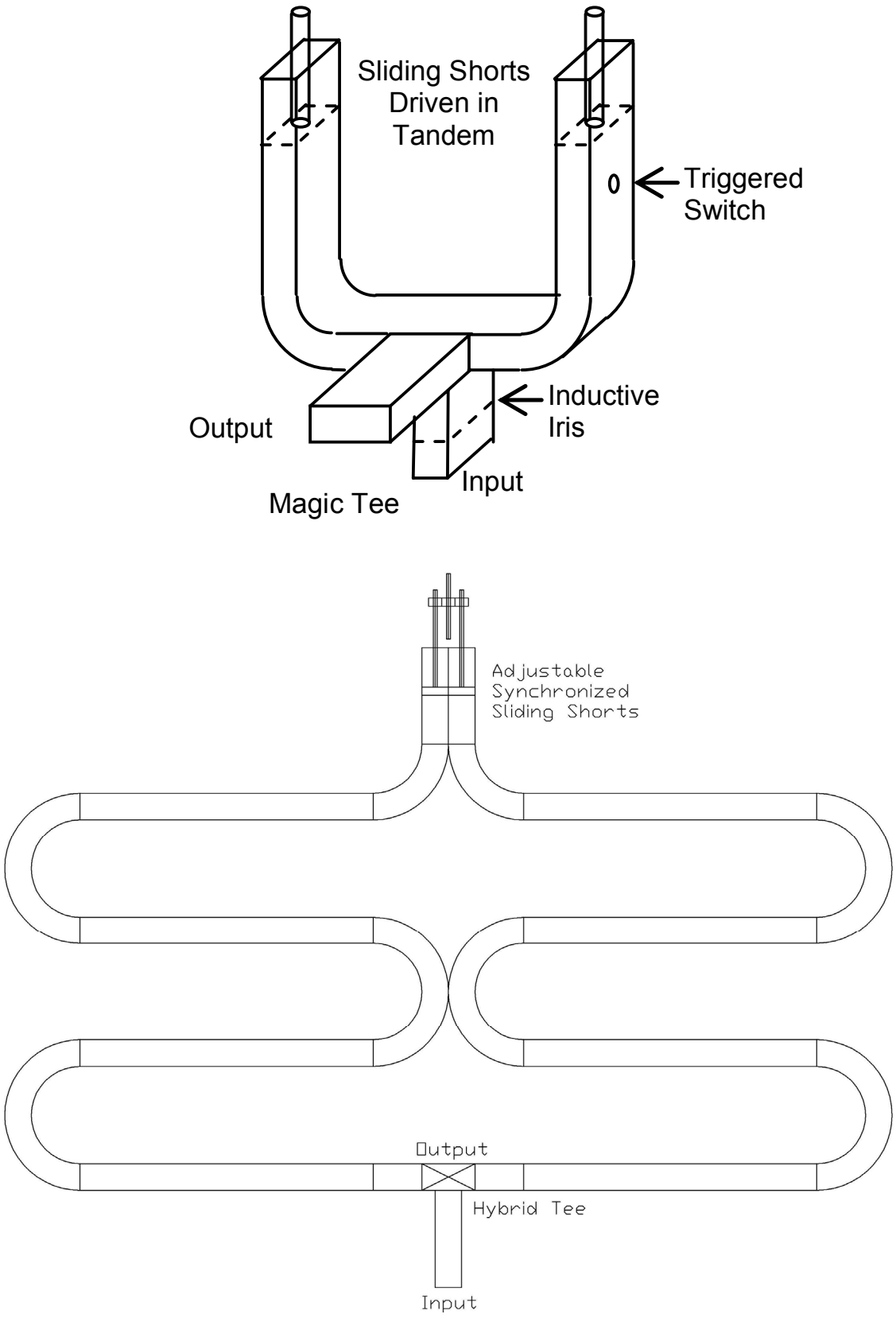

Figure 26. Frequency-tunable Microwave Pulse Compressor concepts.

VI. Conclusions

We have presented data on microwave pulse compression carried out at both low and high power. At high power, we amplified a 2.8 MW source up to 330 MW in the cavity and 51.8 MW at the output. We found a gain of 20.7 dB in the cavity, and 12.7 dB in output. PRFs ranged over 5-160 Hz.

Future work could involve three areas. First one could increase the power with a smoother cavity and by sealing leaks, so one could operate at higher pressure. Second one could design a more compact microwave source, to make the entire system more portable. Third, one could design a frequency-tunable cavity, to allow more flexibility in vulnerability testing.

References

1. R. A. Alvarez, D. P. Byrne, and R. M. Johnson, Prepulse suppression in microwave pulse-compression cavities, *Rev. Sci. Instrum.* 57, October 1986, pp. 2475-2480.

2. R. A. Alvarez, Some properties of microwave resonant cavities relevant to pulse-compression power amplification, *Rev. Sci. Instrum*. 57, October 1986, pp. 2481-2488.

3. P. Yu. Chumerin, A. N. Didenko, S. A. Novikov, and Yu. G. Yushkov, Resonance Pulse Compression as an Effective Method for Generation of UWB High Repetitive Microwave Pulses, in *Ultra-Wideband Short-Pulse Electromagnetics 6*, E. Mokole (ed.), Kluwer Academic Press / Plenum Publishers, 2003, pp. 427-434.

4. Yu. G. Yushkov, V. A. Avgustinovich, S. N. Artemenko, V. L. Kaminsky, S. A. Novikov, V. Razin, P. Yu. Chumerin, "Powerful microwave compressors of RF-pulses," in "Strong Microwaves in Plasmas," Russian Academy of Sciences, Institute of Applied Physics, Nizhny Novgorod, 1996, Vol. 2, pp. 911-925.

5. A. L. Vikharev, A. M. Gorbachev, O. A. Ivanov, V. A. Isaev, S. V. Kuzikov, M. I. Petelin, and J. L. Hirschfield, "Active pulse compression," in "Strong Microwaves in Plasmas," Russian Academy of Sciences, Institute of Applied Physics, Nizhny Novgorod, 2000, Vol. 2, pp. 896-914.

6. D. P. Byrne, Intense Microwave Pulse Propagation Through Gas Breakdown Plasmas in a Waveguide, Ph.D. Thesis, October, University of California Davis, Lawrence Livermore National Laboratory, UCRL-53764, 1986.

7. C. E. Baum, "Compression of Sinusoidal Pulses for High-Power Microwaves," Circuit and Electromagnetic System Design Note 48, March 2004.

8. C. E. Baum, Impedance-Matched Magic Tee, Circuit and Electromagnetic System Design Note 51, March 2006.

9. C. E. Baum, Coupling Ports in Waveguide Cavities for Multiplying fields in Pulse-Compression Systems, Circuit and Electromagnetic System Design Note 52, March 2006

10. D. M. Pozar, *Microwave Engineering*, 2nd edition. New York, Wiley, 1998.

11. A. Andreev, E. G. Farr, and E. Schamiloglu, "Microwave Pulse Compression," Circuit and Electromagnetic System Design Note 57, August, 2008, available for download from the Summa Foundation website, *www.ece.unm.edu/summa/notes*.